applied sciences

MDPI

Article

Surface Characteristics and Cell Adhesion Behaviors of the Anodized Biomedical Stainless Steel

Heng-Jui Hsu [1,2], Chia-Yu Wu [3,4], Bai-Hung Huang [2,5,6], Chi-Hsun Tsai [7], Takashi Saito [7], Keng-Liang Ou [2,8,9,10], Yen-Chun Chuo [2,4], Kuan-Ling Lin [11,*] and Pei-Wen Peng [2,4,*]

1 School of Dentistry, College of Oral Medicine, Taipei Medical University, Taipei 110, Taiwan; d204102004@tmu.edu.tw
2 Biomedical Technology R & D Center, China Medical University Hospital, Taichung 404, Taiwan; T33782@mail.cmuh.org.tw (B.-H.H.); klou@tmu.edu.tw (K.-L.O.); m249108001@tmu.edu.tw (Y.-C.C.)
3 Division of Oral and Maxillofacial Surgery, Department of Dentistry, Taipei Medical University Hospital, Taipei 110, Taiwan; 903027@h.tmu.edu.tw
4 School of Dental Technology, College of Oral Medicine, Taipei Medical University, Taipei 110, Taiwan
5 Implant Academy of Minimally Invasive Dentistry, Taipei 106, Taiwan
6 Asia Pacific Laser Institute, New Taipei City 220, Taiwan
7 Division of Clinical Cariology and Endodontology, Department of Oral Rehabilitation, School of Dentistry, Health Sciences University of Hokkaido, Hokkaido 061-0293, Japan; e526095019@tmu.edu.tw (C.-H.T.); t-saito@hoku-iryo-u.ac.jp (T.S.)
8 Department of Oral Hygiene Care, Ching Kuo Institute of Management and Health, Keelung 203, Taiwan
9 Department of Dentistry, Taipei Medical University-Shuang Ho Hospital, New Taipei City 235, Taiwan
10 3D Global Biotech Inc. (Spin-off Company from Taipei Medical University), New Taipei City 221, Taiwan
11 Division of Family and Operative Dentistry, Department of Dentistry, Taipei Medical University Hospital, Taipei 110, Taiwan
* Correspondence: 150357@h.tmu.edu.tw (K.-L.L.); apon@tmu.edu.tw (P.-W.P.)

Received: 7 August 2020; Accepted: 8 September 2020; Published: 9 September 2020

Abstract: In this study, an electrochemical anodizing method was applied as surface modification of the 316L biomedical stainless steel (BSS). The surface properties, microstructural characteristics, and biocompatibility responses of the anodized 316L BSS specimens were elucidated through scanning electron microscopy, X-ray photoelectron spectroscopy, X-ray diffractometry, transmission electron microscopy, and in vitro cell culture assay. Analytical results revealed that the oxide layer of dichromium trioxide (Cr_2O_3) was formed on the modified 316L BSS specimens after the different anodization modifications. Moreover, a dual porous (micro/nanoporous) topography can also be discovered on the surface of the modified 316L BSS specimens. The microstructure of the anodized oxide layer was composed of amorphous austenite phase and nano-Cr_2O_3. Furthermore, in vitro cell culture assay also demonstrated that the osteoblast-like cells (MG-63) on the anodized 316L BSS specimens were completely adhered and covered as compared with the unmodified 316L BSS specimen. As a result, the anodized 316L BSS with a dual porous (micro/nanoporous) oxide layer has great potential to induce cell adhesion and promote bone formation.

Keywords: 316L biomedical stainless steel; anodization; microstructure; dichromium trioxide; biocompatibility

1. Introduction

Type 316L biomedical stainless steel (BSS) has been used widely in orthopedic implants and bone plates due to its lower cost, higher fracture toughness, superior manufacture properties, accepted biocompatibility, and having the most anti-corrosion properties when in direct contact with biological

fluid [1–3]. Especially in the anti-corrosion performance, it is critical that a surgical implant is not susceptible to corrosion when implanted inside the human body, in order to avoid the chances of infection happening. Unfortunately, if biomedical grade titanium is exposed to hydrogen, nitrogen and oxygen, it is easily contaminated, which may affect the corrosion process of the metal and may impair its use in certain medical procedures [4,5].

Despite the 316L BSS bone plates and implants having proved their long-term clinical success, some situations, such as placing in bone beds with poor quality and quantity, should be improved to integrate faster [6,7]. In addition, BSSs have several disadvantages for use in fracture care such as allergic reactions to the nickel element and a higher modulus of elasticity that causes stress shielding and bone loss, etc. [4,8–11]. To improve these disadvantages of BSSs and then enhance their surface properties and biocompatibility, various surface modification approaches were employed to alter the surface performances of BSSs [12–16]. Tonino et al. [17] have indicated that the formation of a porous oxide layer on the surface of the 316L BSS implants can be utilized in the morphological fixation of the implants to bone through bony ingrowth into the porous microstructure.

Based on the improvement of 316L BSS implants, an electrochemical anodizing process was adopted as a surface treatment method to modify the 316L BSS in this study. Previous studies by our research team have reported that the anodized titanium with a hierarchical porous (micro and nanoporous) surface possessed great potential to enhance cell adhesion ability [18,19]. Accordingly, the potential anodizing method could be utilized to fabricate a promising hierarchical porous surface on the 316L BSS implant to promote biocompatibility. Hou et al. [20] also indicated that the porous oxide surface played a vital role in improving the stress transfer between implant, cortical bone, and cancellous bone for preventing stress-shielding formation. In addition, the modified implant with a porous oxide surface was considered to have outstanding hemocompatibility, biocompatibility, and osseointegration [20–22]. In order to realize the surface properties of the anodized 316L BSS, the surface characteristics and cell adhesion behaviors of the 316L BSS with and without anodizing modification were analyzed in this study. The research results could offer new scientific information in the biomedical fields.

2. Materials and Methods

2.1. Specimens Preparation

The 316L BSS discs with a dimension of 15 mm (diameter) and 1.2 mm (thickness) were used as substrates in this study. The substrates were mechanically ground via different grit papers (600–1200) and polished through diamond abrasives with a particle size of 1 μm. Afterward, the substrates were finished using silicon dioxide abrasives with a particle size of 0.05 μm. Before modification, degreasing and acid pre-pickling of all substrates were done through acetone, with a concentration of 2% ammonium fluoride, a concentration of 2% hydrofluoric acid, and a concentration of 10% nitric acid at 25 °C for 60 s. Subsequently, the substrates were etched in a solution containing nitric acid (4%) and hydrofluoric acid (2%) at 25 °C for 30 s, and were subsequently ultrasonically cleaned with distilled water. After that, the substrates were modified in an anodic polarization with 1 M sulfuric acid and 1 M nitric acid solution at a constant current for 60 s (temperature of 25 °C) (Figure 1). The voltage was kept at 0.5, 1, 3, 5, and 8 V for 5 min. The platinum counter electrode was adopted in the present treatment. The distance between the platinum electrode and substrate was 40 mm.

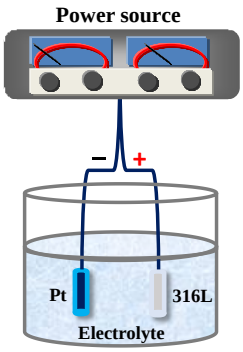

Figure 1. A schematic diagram showing the experimental setup used for surface modification.

2.2. Analysis of the Surface Properties

The surface morphology was analyzed using a JEOL S-5000 field-emission scanning electron microscope (FE-SEM, Tokyo, Japan). The accelerating voltage and emission extracting voltage were kept at 20 kV and around 5 kV, respectively. In addition, surface chemical bonding states were analyzed via Perkin Elmer model PHI 1600 X-ray photoelectron spectroscopy (XPS, Waltham, MA, USA) with an X-ray source of Mg Kα at 250 W. The analyzer is at an angle of 54.7° relative to the X-ray beam. Before detection, the argon ion was utilized to purge the investigated specimens at 3 kV for 5 min. An Au $4f_{7/2}$ peak at 83.8 eV was conducted to calibrate the energy.

2.3. Microstructure Identification

Crystalline structure and phase transformation of the investigated specimens were analyzed using a high-resolution transmission electron microscope (TEM; JEOL-2100, Tokyo, Japan) at an accelerating voltage of 300 kV. Samples for the electron microscope must obviously fit into the holder and hence are usually limited to a disk of a maximum external diameter of approximately 3 mm and a thickness of about 0.5 mm. In this study, the TEM sample was automatically ground using mechanical dimpling down to a thickness of 20 μm. Afterward, an electron transparent area was carefully milled by a Gatan model 691 precision ion polisher (Pleasanton, CA, USA) for observation.

2.4. Cell Response Evaluation

For cell response evaluation, the investigated specimens (n = 3) were subjected to cell culture with osteoblast-like cell line (MG-63, ATCC CRL-1427, Taiwan). The investigated specimens were sealed in the sterile pouch and sterilized with ethylene oxide (3M 8XL, St. Paul, MN, USA). Before the experiment, a mixture solution containing Dulbecco's Modified Eagle Minimum Essential Medium (DMEM; Gibco, Taiwan) and 0.1 M phosphate buffer saline (PBS; Gibco pH 7.4, Taiwan) was used to rinse the modified specimens. Subsequently, the specimens were moved to the polystyrene plate with 24-well and the DMEM culture medium (10% fetal bovine serum, 100 mg/mL streptomycin, and 100 units/mL penicillin) with a cell density of $5 \times 10^4/cm^2$ was seeded onto each specimen surface. Then, the cell seeded specimens were incubated at a temperature of 37 °C with 5% CO_2 for 12 h and 24 h, respectively. After the end of the incubation period, the cells were fixed at a temperature of 25 °C for 1 h through a glutaraldehyde solution with 2% concentration. Specimens were washed twice using PBS solution and dried thoroughly at 30 °C in an oven. Finally, cell morphology and adhesion behavior were examined using the JEOL S-5000 FE-SEM with an accelerating voltage of 20 kV at different magnifications. Before FE-SEM operation, a thickness of 20 nm~30 nm platinum film was coated on the specimen surface to prevent sample charging and provide conductivity. The surface modified 316L BSS implants with the same modification parameters were also subjected to cell culture for cell response evaluation.

3. Results and Discussion

Figure 2 presents the FE-SEM micrographs of the unmodified 316L BSS specimen and 316L BSS specimens following various anodized voltages for 5 min. Figure 2a is the 316L BSS surface without any modification. No porosity feature can be found on the specimen surface, while a porous structure was observed on the 316L BSS surface following various modified voltages, as shown in Figure 2b through Figure 2d. It was found that dual porous (micro/nanoporous) microstructures were formed on the 316L BSS surface when the anodized voltage increased up to 5 V. This feature can also be observed in the modified surface at 8 V for 5 min. The dual porous structure was related to the anodic voltage. The improvement in implant performance is due to the thick oxide layer and porosity because it enhances the adhesion between the artificial bone and genuine bone. In addition, the metallic ion can be restrained by thick oxide film. A similar porous structure can also be found following dipping in the solution of NaOH at high temperature for a long duration [23,24].

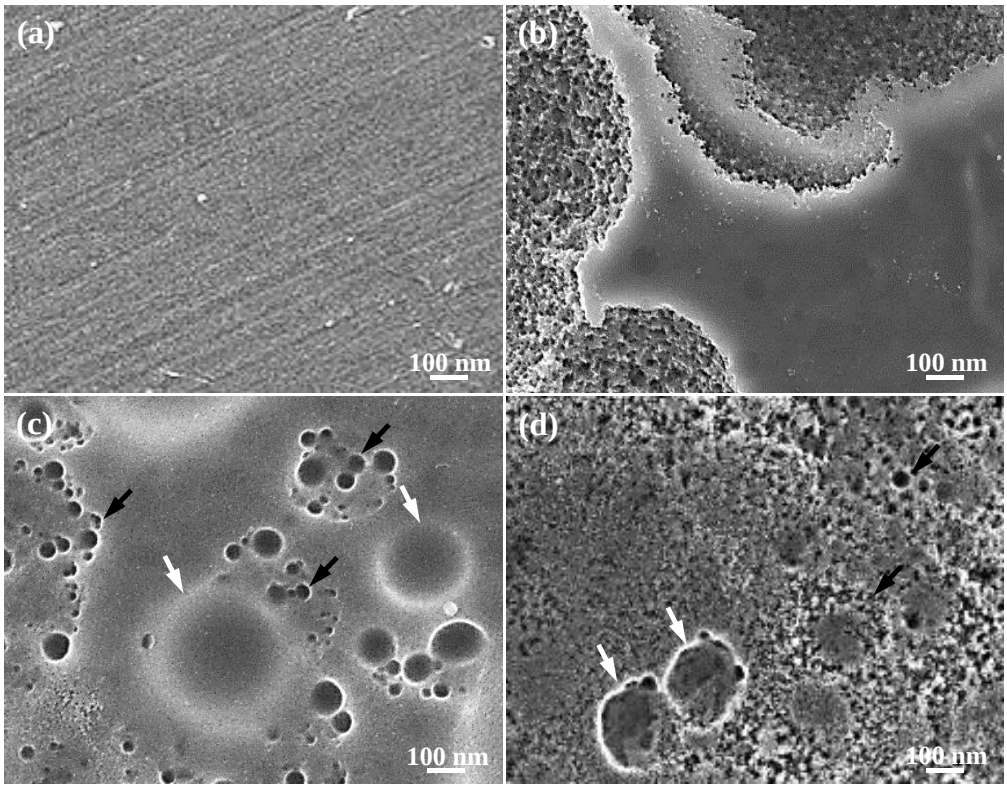

Figure 2. FE-SEM micrographs of the unmodified 316L biomedical stainless steel (BSS) specimen and 316L BSS following various anodized voltages for 5 min: (**a**) unmodified, (**b**) anodized at 3 V, (**c**) anodized at 5 V, and (**d**) anodized at 8 V. (Micropores and nanopores are indicated by white and black arrows, respectively).

Figure 3 shows the XPS spectrum of the 1s orbital of oxygen atom (O 1s), which was taken from the 316L BSS specimen with anodization at 5 V for 5 min. Chemical bonding states relating to O are detected during anodization. After anodizing, the position of O 1s shifted significantly, corresponding to O 1s at 531 eV. The emission peak at ~577.5 eV is attributed to the presence of O atoms or molecules in the interstitial sites. As the voltage raised to 8 V, the emission peak at ~577.5 eV is dominated in the spectrum of O 1 s. The findings revealed that some of O atoms did not form covalent and/or ionic bonds with Cr atoms following the anodization. Some inserted O atoms segregate as functional impurities in the grain boundaries and interstitial sites of the oxide film. It is indicated that enhancement of Cr-O bonding is formed via anodization following various voltages. Accordingly, it reveals that the Cr oxides (Cr_2O_3) were formed on the anodized 316L BSS surface with a higher voltage above 5 V. Similar results were investigated by previous reports [25,26].

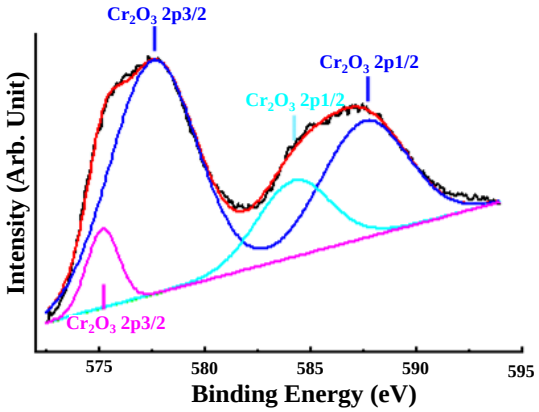

Figure 3. The XPS spectrum of O 1s of the 316L BSS specimen with anodization at 5 V for 5 min.

Figure 4 depicts TEM micrographs of the unmodified 316L BSS and anodized 316L BSS specimens. Figure 4a is a bright-field image of the unmodified 316L BSS, which was taken from the austenite (γ) matrix in the [001] zone under two-beam condition, showing the grain structure within the γ matrix. No other intermetallic compounds or precipitates were detected in the matrix. Figure 4b shows a bright-field micrograph of the anodized 316L BSS specimen at 5 V for 5 min. The figure indicates the formation of different microstructures (as indicated by A and B) in the matrix. The absence of diffraction points from area A reveal the formation of an amorphous structure on the oxidized surface (Figure 4c). From the area B, the pattern with a diffraction ring feature replaces the non-diffraction spots pattern (Figure 4d). It proves that area B belongs to a nanocrystalline structure. Based on the reflection spots corresponding to camera length and *d*-spacings, the precipitate with a nanocrystalline structure was determined to be Cr_2O_3. The microstructural characteristics can also be found in the anodized specimen at 8 V for 5 min. Therefore, the oxide layer microstructure of the anodized 316L BSS with a treatment voltage above 5 V was amorphous γ-phase containing nano-Cr_2O_3. Typically, the formation of an amorphous microstructure must have a high cooling rate [27]. Phase transition during supercooling resulted in the variation of microstructures in the oxide layer.

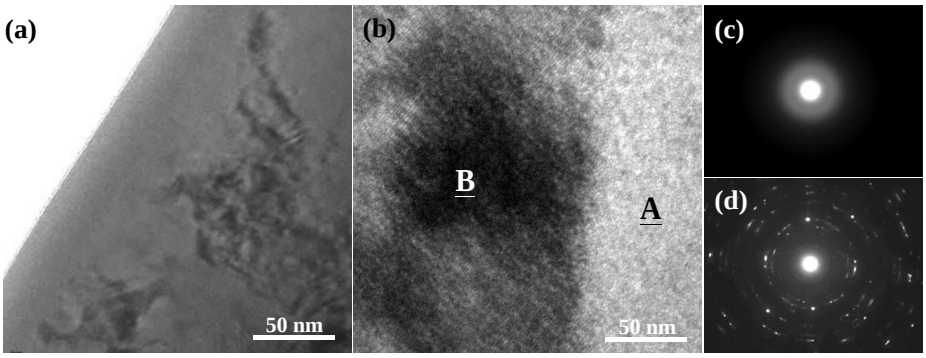

Figure 4. TEM micrographs of the unmodified 316L BSS and anodized 316L BSS specimens. (**a**) Bright-field image of the unmodified 316L BSS specimen, (**b**) bright-field image of the anodized 316L BSS specimen at 5 V for 5 min, (**c**) selected-area diffraction pattern taken from the area **A** in (**b**), and (**d**) selected-area diffraction pattern taken from the area **B** in (**b**).

The FE-SEM investigations of cell morphology on the unmodified 316L BSS specimen and 316L BSS specimen following various modified voltages are displayed in Figure 5. As they were cultured for 12 h, the cells with protruding nuclei were found on the unmodified specimen, although certain cells were well spread, flat, and polygonal, while the cells on the anodized specimens have no clear orientation. The cells were well distributed, strongly attached, and obviously polygonal with no prominent nuclei. After culturing for 24 h, the cells had started to grow along the surface microtracks

on the unmodified 316L BSS specimen. However, it is obvious that the cells were flat attached, elongated, and irregularly networked, revealing that the anodized 316L BSS specimens had greater biocompatibility than unmodified 316L BSS specimen. The roughness surface, such as microporous and/or dual porous topographies as functionalized surface, exhibited a similar cell behavior and response [20,28,29]. Accordingly, cells spread on the anodized 316L BSS specimens, under different culturing periods, revealed strong attachment and biocompatible capability. The cells were fully adapted to the anodized 316L BSS specimens.

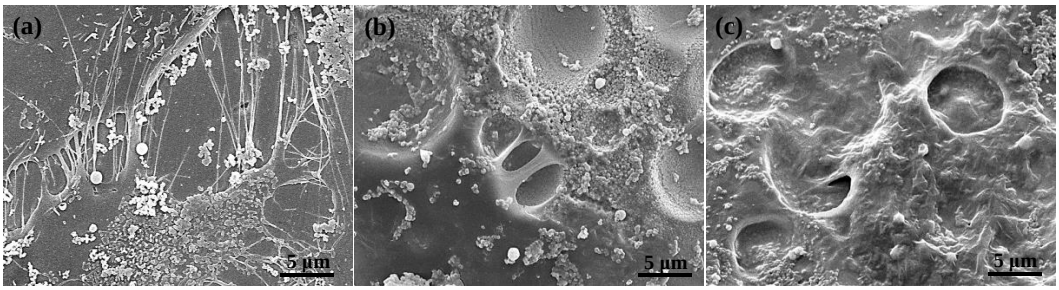

Figure 5. The SEM investigations of osteoblast-like cell (MG-63) morphology on the unmodified 316L BSS specimen and anodized 316L BSS specimens for 24 h incubation: (**a**) unmodified, (**b**) anodized at 5 V for 5 min, and (**c**) anodized at 8 V for 5 min.

As investigated above, the cells spread on the anodized 316L BSS more quickly than on the unmodified 316L BSS. It is well-known that the surface performance of implants must be treated in biocompatible and controlled processing [30]. Implants should have high biocompatibility. To induce and improve the functionality and biocompatibility of implants, it is common a method to modify the implant surfaces. Therefore, metal-based implants such as titanium, titanium alloys, as well as BSSs, are recommended for coating processes on blood contact implants. The blood cells' interaction on different implants including micoporous and/or nanoporous surfaces have been clearly investigated by previous studies [31–33]. When roughness (Ra) is in the range of 0.2 mm~0.5 mm, the cell adhesion ability of the rough surfaces is higher than that of the smooth surfaces [23]. In addition, nitrided implants exhibit higher human salivary albumin adsorption, indicating that human albumin has a high affinity for implants [12]. Hence, importantly, surface characteristics can be modified by surface functionalization and directly influence biocompatibility. Figure 6 also presents the cell culture of the 316L BSS implant with anodization treatment. The cells exhibited good adhesion behavior on the oxidized surface with a porous structure. Therefore, it is believed that implant surfaces with porosity can enhance cell activity. Finally, more investigations should be carried out to provide scientific information concerning surface properties and in vivo biocompatibility in the presence of anodized 316L BSS.

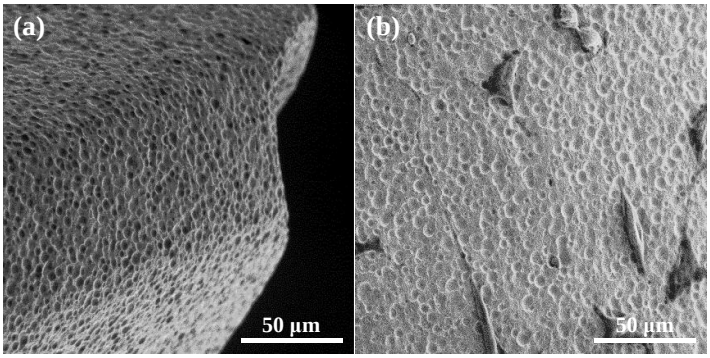

Figure 6. The cell culture of MG 63 on the anodized 316L BSS implant (5 V for 5 min) for 24 h: (**a**) the anodized surface before cell culture and (**b**) the anodized surface after cell culture.

4. Conclusions

The effectiveness of anodization on the surface functionalization of 316L BSS has been examined in the present study. The oxide layer, including the nanostructure, was processed by anodization treatment. The nano-Cr_2O_3 oxides were formed in the oxide layer. A $\gamma \rightarrow$ oxide ordering transition would occur in the γ matrix during anodization. The microstructure of the anodized 316L BSS comprised γ-phase containing nano-Cr_2O_3 oxides. The oxide layer, including the nanostructure, is a critical factor in inducing the biocompatibility of the 316L BSS. Thus, the phase transformation of the 316L BSS following anodization can enhance and induce an increase in the biocompatibility and osseointegration potential.

Author Contributions: Writing—original draft, H.-J.H.; Investigation, C.-Y.W.; Data curation, Y.-C.C. and C.-H.T.; Validation, B.-H.H.; Supervision, T.S. and K.-L.O.; Writing—review and editing, K.-L.L. and P.-W.P. All authors have read and agreed to the published version of the manuscript.

Funding: This research received no external funding.

Conflicts of Interest: The authors report no conflicts of interest in this work.

References

1. Chikarakara, E.; Naher, S.; Brabazon, D. Process mapping of laser surface modification of AISI 316L stainless steel for biomedical applications. *Appl. Phys. A-Mater.* **2010**, *101*, 367–371. [CrossRef]
2. Martinesi, M.; Bruni, S.; Stio, M.; Treves, C.; Bacci, T.; Borgioli, F. Biocompatibility evaluation of surface-treated AISI 316L austenitic stainless steel in human cell cultures. *J. Biomed. Mater. Res. A* **2007**, *80*, 131–145. [CrossRef]
3. Stio, M.; Martinesi, M.; Treves, C.; Borgioli, F. Cultures and co-cultures of human blood mononuclear cells and endothelial cells for the biocompatibility assessment of surface modified AISI 316L austenitic stainless steel. *Mater. Sci. Eng. C Mater. Biol. Appl.* **2016**, *69*, 1081–1091. [CrossRef] [PubMed]
4. Eliaz, N. Corrosion of Metallic Biomaterials: A Review. *Materials* **2019**, *12*, 407. [CrossRef]
5. Manam, N.S.; Harun, W.S.W.; Shri, D.N.A.; Ghani, S.A.C.; Kurniawan, T.; Ismail, M.H.; Ibrahim, M.H.I. Study of corrosion in biocompatible metals for implants: A review. *J. Alloys Compd.* **2017**, *701*, 698–715. [CrossRef]
6. Seligson, D.; Mehta, S.; Mishra, A.K.; FitzGerald, T.J.; Castleman, D.W.; James, A.H.; Voor, M.J.; Been, J.; Nawab, A. In vivo study of stainless steel and Ti-13Nb-13Zr bone plates in a sheep model. *Clin. Orthop. Relat. Res.* **1997**, *343*, 213–223. [CrossRef]
7. Disegi, J.A.; Eschbach, L. Stainless steel in bone surgery. *Injury* **2000**, *31* (Suppl. 4), 2–6. [CrossRef]
8. Niinomi, M.; Nakai, M.; Hieda, J. Development of new metallic alloys for biomedical applications. *Acta Biomater.* **2012**, *8*, 3888–3903. [CrossRef]
9. Yang, K.; Ren, Y.B. Nickel-free austenitic stainless steels for medical applications. *Sci. Technol. Adv. Mater.* **2010**, *11*. [CrossRef]
10. Hassanin, H.; Al-Kinani, A.A.; ElShaer, A.; Polycarpou, E.; El-Sayed, M.A.; Essa, K. Stainless steel with tailored porosity using canister-free hot isostatic pressing for improved osseointegration implants. *J. Mater. Chem. B* **2017**, *5*, 9384–9394. [CrossRef]
11. Heary, R.F.; Parvathreddy, N.; Sampath, S.; Agarwal, N. Elastic modulus in the selection of interbody implants. *J. Spine Surg.* **2017**, *3*, 163–167. [CrossRef] [PubMed]
12. Lin, L.H.; Chen, S.C.; Wu, C.Z.; Hung, J.M.; Ou, K.L. Microstructure and antibacterial properties of microwave plasma nitrided layers on biomedical stainless steels. *Appl. Surf. Sci.* **2011**, *257*, 7375–7380. [CrossRef]
13. Huang, C.F.; Chiang, H.J.; Lan, W.C.; Chou, H.H.; Ou, K.L.; Yu, C.H. Development of silver-containing austenite antibacterial stainless steels for biomedical applications Part I: Microstructure characteristics, mechanical properties and antibacterial mechanisms. *Biofouling* **2011**, *27*, 449–457. [CrossRef]
14. Ou, K.L.; Chu, J.S.; Hosseinkhani, H.; Chiou, J.F.; Yu, C.H. Biomedical nanostructured coating for minimally invasive surgery devices applications: Characterization, cell cytotoxicity evaluation and an animal study in rat. *Surg. Endosc.* **2014**, *28*, 2174–2188. [CrossRef] [PubMed]
15. Wu, C.M.; Lu, Y.J.; Chen, S.Y.; Wen, S.C.; Wu, C.H.; Liao, P.B.; Ou, K.L.; Chou, H.H. Surface characterization and thermomechanical behavior of nanostructured-gold layer for biomedical applications. *J. Alloys Compd.* **2019**, *782*, 1114–1120. [CrossRef]

16. Bekmurzayeva, A.; Duncanson, W.J.; Azevedo, H.S.; Kanayeva, D. Surface modification of stainless steel for biomedical applications: Revisiting a century-old material. *Mater. Sci. Eng. C Mater.* **2018**, *93*, 1073–1089.
17. Tonino, A.J.; Davidson, C.L.; Klopper, P.J.; Linclau, L.A. Protection from stress in bone and its effects. Experiments with stainless steel and plastic plates in dogs. *J. Bone Jt. Surg. Br.* **1976**, *58*, 107–113. [CrossRef]
18. Lan, W.C.; Wang, C.H.; Huang, B.H.; Cho, Y.C.; Saito, T.; Huang, C.C.; Huang, M.S. Fabrication of a Promising Hierarchical Porous Surface on Titanium for Promoting Biocompatibility. *Appl. Sci.* **2020**, *10*, 1363. [CrossRef]
19. Chen, C.S.; Tsao, Y.L.; Wang, D.J.; Ou, S.F.; Cheng, H.Y.; Chiang, Y.C.; Ou, K.L. Research on cell behavior related to anodized and hydrothermally treated titanium surface. *Appl. Surf. Sci.* **2013**, *271*, 1–6. [CrossRef]
20. Hou, P.J.; Ou, K.L.; Wang, C.C.; Huang, C.F.; Ruslin, M.; Sugiatno, E.; Yang, T.S.; Chou, H.H. Hybrid micro/nanostructural surface offering improved stress distribution and enhanced osseointegration properties of the biomedical titanium implant. *J. Mech. Behav. Biomed.* **2018**, *79*, 173–180. [CrossRef]
21. Wu, C.M.; Liu, C.M.; Ou, K.L.; Chiang, H.J.; Sugiatno, E.; Wu, C.H.; Yen, H.J.; Chou, H.H. Nanostructured titanium dioxide layer combined with reactive functional groups as a promising biofunctional surface for biomedical applications. *Ceram. Int.* **2019**, *45*, 9712–9718. [CrossRef]
22. Hsu, L.C.; Lan, W.C.; Ou, K.L.; Chou, H.H.; Wen, C.C.; Liu, C.M.; Endo, K.; Huang, M.S.; Huang, H.F. Fabrication of biomolecules coated nanostructured oxide layer to facilitate cell adhesion and proliferation for improving osseointegration. *Ceram. Int.* **2019**, *45*, 21941–21946. [CrossRef]
23. Ji, J.; Tan, Q.; Fan, D.Z.; Sun, F.Y.; Barbosa, M.A.; Shen, J. Fabrication of alternating polycation and albumin multilayer coating onto stainless steel by electrostatic layer-by-layer adsorption. *Colloids Surf. B Biointerfaces* **2004**, *34*, 185–190. [CrossRef] [PubMed]
24. Vallet-Regi, M.; Izquierdo-Barba, I.; Gil, F.J. Localized corrosion of 316L stainless steel with SiO_2-CaO films obtained by means of sol-gel treatment. *J. Biomed. Mater. Res. Part A* **2003**, *67*, 674–678. [CrossRef]
25. Harun, W.S.W.; Asri, R.I.M.; Romlay, F.R.M.; Sharif, S.; Jan, N.H.M.; Tsumori, F. Surface characterisation and corrosion behaviour of oxide layer for SLMed-316L stainless steel. *J. Alloys Compd.* **2018**, *748*, 1044–1052. [CrossRef]
26. Mandrino, D.; Godec, M.; Torkar, M.; Jenko, M. Study of oxide protective layers on stainless steel by AES, EDS and XPS. *Surf. Interface Anal.* **2008**, *40*, 285–289. [CrossRef]
27. Fan, X.W.; Lin, L.J.; Dalsin, J.L.; Messersmith, P.B. Biomimetic anchor for surface-initiated polymerization from metal substrates. *J. Am. Chem. Soc.* **2005**, *127*, 15843–15847. [CrossRef]
28. Chen, S.L.; Lin, M.H.; Huang, G.X.; Wang, C.C. Research of the recast layer on implant surface modified by micro-current electrical discharge machining using deionized water mixed with titanium powder as dielectric solvent. *Appl. Surf. Sci.* **2014**, *311*, 47–53. [CrossRef]
29. Tsai, M.H.; Haung, C.F.; Shyu, S.S.; Chou, Y.R.; Lin, M.H.; Peng, P.W.; Ou, K.L.; Yu, C.H. Surface modification induced phase transformation and structure variation on the rapidly solidified recast layer of titanium. *Mater. Charact.* **2015**, *106*, 463–469. [CrossRef]
30. Mazumder, M.M.; De, S.; Trigwell, S.; Ali, N.; Mazumder, M.K.; Mehta, J.L. Corrosion resistance of polyurethane-coated Nitinol cardiovascular stents. *J. Biomater. Sci. Polym. E* **2003**, *14*, 1351–1362. [CrossRef]
31. Chang, J.C.; Oshida, Y.; Gregory, R.L.; Andres, C.J.; Barco, T.M.; Brown, D.T. Electrochemical study on microbiology-related corrosion of metallic dental materials. *Bio-Med. Mater. Eng.* **2003**, *13*, 281–295.
32. Chiang, H.J.; Chou, H.H.; Ou, K.L.; Sugiatno, E.; Ruslin, M.; Abd Waris, R.; Huang, C.F.; Liu, C.M.; Peng, P.W. Evaluation of Surface Characteristics and Hemocompatibility on the Oxygen Plasma-Modified Biomedical Titanium. *Metals* **2018**, *8*, 513. [CrossRef]
33. Park, J.Y.; Davies, J.E. Red blood cell and platelet interactions with titanium implant surfaces. *Clin. Oral Implant. Res.* **2000**, *11*, 530–539. [CrossRef] [PubMed]

© 2020 by the authors. Licensee MDPI, Basel, Switzerland. This article is an open access article distributed under the terms and conditions of the Creative Commons Attribution (CC BY) license (http://creativecommons.org/licenses/by/4.0/).